Three-Dimensional Numerical Simulation of a Failed Coronary Stent Implant at Different Degree of Residual Stenosis. Part II: apparent viscosity and wall permeability.

Andrea Boghi[a], Ivan Di Venuta[b], Fabio Gori[b,*]

[a] School of Water, Energy and Agrifood, Cranfield University, Cranfield, Bedfordshire MK43 0AL, United Kingdom,

[b] Department of Industrial Engineering, University of Rome "Tor Vergata", Via del Politecnico 1, 00133 Rome, Italy.

[*] Corresponding Author, gori@uniroma2.it

Abstract

The influence of the degree of residual stenosis (DOR) on the hemodynamics inside coronary arteries is investigated through three-dimensional (3D) numerical simulations. The vascular wall permeability is investigated and the effect of the non-Newtonian viscosity discussed. The results agree in predicting an abrupt increase in wall permeability above 45% DOR, indicating that the implant could lead to a massive restenosis. This behavior is considered due to the shift of the regions interested by low and oscillatory WSS, from the zone adjacent to the struts towards the center of the stent meshes.

Keywords: stent, stenosis, blood viscosity, Optical Density, Relative Residence Time.

Nomenclature

Latin

Ca	Casson number.
DOR	degree of restenosis.
M	amount of dye deposited for unit of surface, $nmol/cm^2$.
MGS	module of gradient stress, $dyne/cm^3$.
OD	optical density.
OSI	oscillatory shear index.
p	static pressure, Pa.
r	radial coordinate, m.
R	radius of cylinder, m.
R_0	minimum radius for which the blood behaves as a liquid, m.
R_e	Reynolds number.
R_{max}	maximum radius, m.
R_{min}	minimum radius, m.
$[S]$	rate of the strain tensor, s^{-1}.
RRT	relative residence time, Pa^{-1}.
$TAWSS$	time averaged wall shear stress magnitude, Pa.
$\vec{v}$	fluid velocity, m/s.
u_m	mean velocity, m/s.

1

WSS	wall shear stress, $dyne/cm^2$.	
WSSG	spatial gradient of wall shear stress, $dyne/cm^3$.	
Greek		
α	absorption coefficient, $cm^2/nmol$.	
$\dot{\gamma}$	shear rate, s^{-1}.	
μ	dynamic viscosity, $Pa \cdot s$.	
μ_∞	asymptotic Newtonian viscosity, $Pa \cdot s$.	
$\xi = r/R$	dimensionless radial coordinate.	
ρ	density, kg/m^3.	
τ_0	yield stress, N/m^2.	

Introduction

Cardiovascular diseases, in particular atherosclerosis, are the leading cause of death in the western world, accounting for the 50% of deaths occurring each year. A strong connection between cardiovascular diseases, such as atherosclerosis, and particular hemodynamic conditions, such as low and oscillatory wall shear stress (WSS) and stagnation of blood flow, has been suggested in [1-3].

Over the last few decades the use of Computational Fluid Dynamics (CFD) in the biomedical field has received an increasing attention [4-5]. Two (2D) and three-dimensional (3D) CFD simulations have been performed in stented arteries in order to investigate the effect of the design, such as the shape of the strut section, [6], and its geometry near the curvatures, [7]. LaDisa et al., [8], investigated how the 3D geometric parameters could influence the neointimal proliferation. Duraiswamy et al., [9], analyzed the correlation between platelet deposition and stent geometry. Gori and coworkers investigated numerically the wall permeability and the non-Newtonian behavior of the blood, [10-12]. To the best of the authors' knowledge, it seems that the influence of the degree of residual stenosis (DOR) has been investigated only in [12], where the blood flow in two models of carotid artery, completely restored after the stent implantation and with 30% DOR, has been analyzed, and in the first paper of this work [13].

The wall permeability has been investigated in the last few decades, both experimentally and numerically [14-17]. For macromolecules, such as LDL, a high endothelial permeability may be associated with the development of atherosclerotic lesions. The spatial variation of macromolecular permeability can be assessed by Evans blue dye (EBD), [18-19]. The optical density (OD) is a parameter evaluating the endothelial permeability. Several studies have been performed in order to obtain a direct relation between fluid dynamic parameters, i.e. WSS and its gradient, and OD [17-21].

The non-Newtonian behavior in CFD studies of stented coronary arteries has been investigated in the literature [22-23], but its influence on hemodynamics in non-completely restored coronary arteries has not been studied yet. A strong correlation between blood viscosity and cardiovascular events has been evidenced, [24]. Indeed, blood viscosity is higher in patients who experienced cardiovascular diseases or who are possibly

subjects to them. Hyper-viscosity and turbulent blood flow activate platelet that explains the distribution of lesions throughout the body. Moreover, HDL cholesterol, which assumes a protective role with respect to atherosclerotic phenomena, has been shown experimentally to appear at lower viscosity values [25]. Therefore, the viscosity is a fundamental parameter to be taken into account.

This paper is the second of a series of two. The first one [13] has investigated the influence of the degree of residual stenosis (DOR) on the fluid dynamics and the shear stresses acting on the stent and the artery wall. The present paper studies the wall permeability and the influence of the non-Newtonian behavior on the blood flow.

1. **Geometry and Computational Grid**

The stent geometry [26] is reconstructed with the commercial software SOLIDWORKS 2010. The vessel wall is modeled as a cylinder with circular section and the wall is considered to be rigid, which is a reasonable assumption since the stent increases the rigidity of the wall. The vessel has a diameter of 2.6 mm, according to [8], and the thickness of the stent is 0.1 mm, according to [27]. The length of the stent is 15 mm.

The other geometries investigated for the simulation of the residual stenosis have a choking in the middle section, with a radius respectively of 1.09 mm, 0.96 mm, 0.89 mm, 0.82 mm, 0.74 mm, 0.65 mm and 0.45 mm, corresponding to 30%, 45%, 52.5%, 60%, 67.5%, 75% and 90% DOR, defined as

$$\text{DOR}(\%) = 100 \left(1 - \left(\frac{R_{\min}}{R_{\max}} \right)^2 \right) \tag{1}$$

The present paper investigates additional values of DOR, i.e. 45%, 52.5%, 67.5%, 75%, compared to those shown in [13], to better understand the influence of DOR on the endothelial permeability.

The blood is considered as an incompressible non-Newtonian fluid, with $\rho = 1060 \text{ kg·m}^{-3}$, obeying to the Casson model [28]. In the steady-state simulations a mean velocity of 0.16 m/s is prescribed for the Casson velocity profile on the inlet, while the pulsatile velocity profile, in the transient simulations, is modeled with the Womersley-Evans theory [29].

2. **Hemodynamic variables**

The non-Newtonian blood is modeled with the Casson relation [28]

$$\mu(\dot{\gamma}) = \left(\mu_\infty + 2\frac{\sqrt{\tau_0 \mu_\infty}}{\sqrt{\dot{\gamma}}} + \frac{\tau_0}{\dot{\gamma}} \right) \tag{2}$$

where τ_0, the yield stress, and μ_∞, the asymptotic Newtonian viscosity, are both functions of the hematocrit.

The difficulty in using the Casson model in a numerical scheme lies in the fact that the function diverges at the zero shear rate limit. In order to avoid this, the regularization technique proposed in [30] has been used and the viscosity expression becomes

$$\mu(\dot{\gamma}) = \left(\mu_\infty + 2\sqrt{\frac{\tau_o}{\dot{\gamma}}\mu_\infty} \left(1 - e^{-\sqrt{\frac{\dot{\gamma}}{\gamma_0}}} \right) + \frac{\tau_o}{\dot{\gamma}} \left(1 - e^{-\sqrt{\frac{\dot{\gamma}}{\gamma_0}}} \right)^2 \right) \tag{3}$$

which, at zero shear rate, becomes

3

$$\mu(0) = \mu_0 = \left(\mu_\infty + 2\sqrt{\frac{\tau_0}{\dot{\gamma}_0}\mu_\infty} + \frac{\tau_0}{\dot{\gamma}_0} \right) \tag{4}$$

and the parameters are $\tau_0 = 0.01 \text{Pa}$ and $\mu_\infty = 0.0033 \text{Pa} \cdot \text{s}$, according to [11,31]. In this study, we assume $\mu_0 = 100\mu_\infty$. The corresponding value of $\dot{\gamma}_0$ can be derived from Eq. (4). The Casson viscosity versus the share rate is reported in Fig. 1.

The wall shear stress (WSS) is the tangential drag force produced by the blood moving across the endothelial surface and is defined as

$$\overrightarrow{WSS} = 2\mu(\dot{\gamma}) \left[[S] \cdot \hat{n} - \left(\hat{n}^T \cdot [S] \cdot \hat{n} \right) \hat{n} \right]_{wall} \tag{5}$$

The absolute value of the WSS is defined as $WSS = \left\| \overrightarrow{WSS} \right\|$. The unit of measurement is dyne·cm^{-2}. The physiological range for the mean WSS value is of 5-70 dyne·cm^{-2} [32-34].

The spatial gradient of the wall shear stress (WSGG) [35], and its absolute value MGS (module of gradient stress), are defined as

$$[WSSG] = \left[\nabla \overrightarrow{WSS} \right] \tag{6}$$

$$MGS = \sqrt{[WSSG]:[WSSG]} \tag{7}$$

High values of MGS are related to restenosis, but their range has not been established yet.

The OD is an important variable in determining the permeability of the wall. There is a relationship between the accumulation of EBD and the OD, indicative of high endothelial permeability, [17],

$$OD = 2M\alpha \tag{8}$$

An empirical expression of OD, depending on both MGS and WSS, is

$$OD = 1.2 WSS^{-0.11} MGS^{0.044} \tag{9}$$

The physiological values of the OD are between 0.9 and 1.3. The accumulation of EBD is highly variable in different regions, so the OD can only be used as a comparative parameter.

The oscillatory shear index (OSI), introduced by Ku et al. [32], is defined as:

$$OSI = 0.5 \left(1 - \left| \int_0^T \overrightarrow{WSS} dt \right| \Big/ \int_0^T WSS\, dt \right) \tag{10}$$

The OSI indicates the regions interested by the inversion of the WSS direction during the cardiac cycle. Its value can vary from zero, without change of direction, to 0.5 for a complete inversion. Areas with high OSI are particularly prone to develop of atherosclerotic lesions [36].

The time Averaged Wall Shear Stress magnitude (TAWSS) is defined as

$$TAWSS = \frac{1}{T} \int_0^T WSS\, dt \tag{11}$$

and can be used to compare the cumulative effects of WSS over an entire cardiac cycle.

The relative residence time (RRT), introduced in [16],

$$RRT = \left[(1 - 2 \cdot OSI) \cdot TAWSS \right]^{-1} = \left[\frac{1}{T} \left| \int_0^T \overrightarrow{WSS} dt \right| \right]^{-1} \tag{12}$$

identifies the regions subjected to stagnant flow. The RRT is higher in the regions of the endothelium, which are more prone to cells and macromolecules infiltration, but gives only a qualitative evaluation of the residence time of the fluid close to the wall.

4. Steady state simulations

A steady state mean velocity of 0.16 m/s is assumed, [35]. The associated Reynolds number is about 132, i.e. the flow is laminar, and a Casson velocity profile is assumed [28].

The steady state velocity $u_s(\xi)$ profile is

$$\frac{u_s(\xi)}{u_m} = \begin{cases} 2 \dfrac{\left(21\left(1 - \xi^2\right) - 56\xi_0\left(1 - \xi^{\frac{3}{2}}\right) + 42\xi_0\left(1 - \xi\right) \right)}{\left(21 - 48\sqrt{\xi_0} + 28\xi_0 - \xi_0{}^4 \right)} & \text{if } \xi \geq \xi_0 \\[4mm] 2 \dfrac{\left(21 - 7\xi_0{}^2 + 42\xi_0 - 56\sqrt{\xi_0} \right)}{\left(21 - 48\sqrt{\xi_0} + 28\xi_0 - \xi_0{}^4 \right)} & \text{if } \xi < \xi_0 \end{cases} \tag{13}$$

where ξ_0 depends on the following non-linear relationship

$$Ca = \frac{168\xi_0}{\left(21 - 48\sqrt{\xi_0} + 28\xi_0 - \xi_0{}^4 \right)} \tag{14}$$

and the fluid moves as a solid block if $\xi < \xi_0$.

The Casson number, Ca, is defined as

$$Ca = \frac{2R\tau_0}{\mu_\infty u_m} \tag{15}$$

which is an index of the non-Newtonian character. In steady state $\xi_0 = 0.005$, which makes the non-Newtonian effect not important in the steady state. Further on, the steady state velocity profile, Eq. (13), is essentially a parabolic profile, as stated in [13]. However, as will be shown later, the non-Newtonian effect will be important in the unsteady state.

5. Results

Figures 2-4 show the results of the apparent viscosity at three time steps, i.e. t=0.3 s (diastole), t=0.4 s and t=0.6 s (systole), on the periodic face of the stents with different DOR, i.e. 0%, 30%, 60% and 90%. Because of the steep variation of the shear rate, the numerical results are reported as the logarithm of the viscosity. In a Casson fluid, the viscosity is inversely proportional to the shear rate, therefore, the non-Newtonian behavior can be significant only in slow-flow conditions. In a rigid tube the shear rate is higher where the pipe diameter is smaller and vice-versa. Therefore, the apparent viscosity is smaller in correspondence to the stenosis and greater where the flow rate is lower. From the results observed in [10-13]

it is possible to infer that the presence of the stent reduces the shear rate, since the WSS, proportional to this variable, is reduced as well.

Figure 2 reports the viscosity profile in the diastolic phase, at t=0.3 s. Figure 2a shows the result for 0% DOR, which is higher at the center of the pipe, in correspondence of the low shear rate, caused by the pulsatile nature of the flow. The viscosity assumes another peak value at a distance from the wall corresponding to one third of the radius, due to the rheology of the blood. As far as the effect of 30% DOR is concerned, Fig. 2b, the apparent viscosity has a trend fairly similar to the case without stenosis, except slightly before and after the stenosis, particularly at the center of the vessel, where the viscosity tends to decrease. This effect is more evident for the cases with 60% DOR, Fig. 2c. As far as the 90% DOR is concerned, Fig. 2d, the apparent viscosity tends to decrease in correspondence to the neck, while downstream the stenosis the higher viscosity is concentrated close to the vessel wall.

Figure 3 shows the viscosity patterns at t=0.4 s, corresponding to the central time-peak of the flow rate. In absence of residual stenosis, 0% DOR of Fig. 3a, the high viscosity is concentrated on the center of the pipe, in correspondence to the low shear rate regions. In this case there is no secondary peak. For 30% DOR, Fig. 3b, the viscosity at the center of the pipe decreases while it assumes a peak just downstream the chocking, where the velocity starts gradually to decrease. As far as the 60% DOR is concerned, Fig. 3c, the field upstream the stenosis is fairly similar to the previous case, but the viscosity decreases in correspondence to the stenosis, where it shows a peak, just after the necking, while downstream the stenosis it assumes lower values, even on the center of the vessel. For 90% DOR, Fig, 3d, these effects are more pronounced, and a peak near the vessel wall is visible.

Similar considerations can be made from the observation of Fig. 4, which shows the viscosity pattern in the systole, t=0.6 s. The differences are small compared to the previous cases, but the viscosity values are smaller because of the higher flow rate, and the secondary peak appears for DOR equal to 60%, Fig. 4c. According to the Casson model, the areas of high viscosity correspond to higher erythrocytes concentrations. The results at different DOR, Figs. 2-4, show that the stenosis increases the erythrocytes concentration towards the wall, which is not a pathological situation, as the erythrocyte can move close to the wall in the diastole, as shown in Fig. 2. However, the presence of the stenosis increases the time spent by the red blood cells close to the wall, which can lead to pathological conditions.

As far as the OD is concerned, Figures 5-7 show the results for the average OD at different time steps t=0.3 s (diastole), t=0.4 s, t=0.6 s (systole). The OD results are averaged over the vessel perimeter.

Figure 5 shows the OD pattern in diastole, t=0.3 s, for 0%, 30%, 60% and 90% DOR. In the area of the vascular wall, the OD assumes physiological values before the stent. In presence of the stent, the OD increases assuming typical patterns with peaks and valleys, corresponding respectively to slices intersecting mostly the struts and the intra-strut areas. The OD assumes a peak where the WSS assumes very low values. The OD values are higher in diastole because of the lower velocity and the presence of stenosis seems to have no effect, except for DOR equal to 90%.

At t=0.4 s, Fig. 6, the OD starts decreasing in correspondence to the necking, due to the very high MGS, while downstream it assumes a different pattern, depending on the severity of the DOR. In particular, it seems that for DOR greater than 60% the OD pattern assumes a peak downstream the stenosis, which moves along the axis with the increasing DOR, in correspondence to the end of the wide recirculation region. For 90% DOR the peak is not visible in the Figure 6, which is due to the fact that for higher DOR, the recirculation region is longer. In this case the local flow is always directed upstream and the WSS direction does not change. Moreover, the WSS is spatially more uniform, which contributes to a reduction of MGS and permeability. For 30% DOR the OD returns to physiological values downstream the stenosis.

In the systole, t=0.6 s, Fig. 7 shows that the most relevant DOR are 0%, 30%, 52.5%, 60%, 67.5% and 90%. At this instant of time, the OD assumes the lowest average values upstream the stenosis because of the highest velocity reached by the blood flow during the cardiac cycle. Downstream the stenosis, even for 52.2% DOR, the local recirculation regions are formed in correspondence to the meshes. Here the OD assumes higher values. For 67.5% DOR a peak in correspondence to the end of the stent is shown, and a wide recirculation region closes. The last peak visible in Fig. 7 is for 67.5% DOR, while for 75% and 90% DOR the recirculation region is longer than the domain length.

The OSI, defined by Eq. (10), measures the WSS deviation from its mean direction and is reported in Fig. (8), for different DOR. Although it is possible to define the OSI for all spatial directions, the change in the mean flow direction is the significant one. Figure 8a presents the results for the case without stenosis. The areas exposed to the non-zero OSI are located near the struts and close to the points with greater curvature, while in the intra-struts areas the values approach zero. Since the OSI values which trigger atherosclerosis span between 0.1 and 0.5 [32, 37], the case without residual stenosis represents a safe scenario, as there are few areas in which the OSI assumes these values.

Figures 8b, c, d report the OSI values for 52.5%, 60% and 67.5% DOR. The OSI assumes greater values, in the range 0.2-0.5, in areas where the fluid is detached from the wall and where, consequently, a recirculation region is present. This is evident at the center of each mesh. Figure 8e shows that, for the greatest DOR investigated, 90%, the OSI assumes hazardous values mostly at the beginning and the end of the recirculation zone. In these two regions the OSI trend is similar to that without residual stenosis, but the WSS vectors are oriented in the direction opposite to the main flow.

The RRT measures the relative time spent by the fluid during the flow in a certain region. This parameter assumes higher values where the OSI is closer to 0.5 and TAWSS is small, therefore RRT allows identifying low and oscillating WSS regions, which are deemed to indicate areas prone to develop atherosclerosis. The RRT increases where the stent is present and decreases on the vessel wall, because it is inversely proportional to TAWSS, which is smaller in proximity of the stent.

Figure 9 reports the RRT versus the axial length for several DOR, 0%, 52.2%, 60%, 67.5%, 75% and 90%. The RRT increases, downstream the stenosis, for 52.2% DOR, because of the local recirculation in correspondence to the center of the mesh. For 60% DOR, the RRT beyond the stenosis assumes higher values than for 52.2% DOR, except in a region immediately downstream the first peak, due to the detachment of the

fluid stream. For 67.5% and 75% DOR, RRT increases with a peak moving along the axial length, which is due to the stable recirculation region downstream the stenosis, whose width is proportional to the DOR. In these condition the local flow is always directed upstream and therefore the WSS direction does not change, except close to the struts. Moreover, the WSS field is more uniform, which contributes to a reduction of MGS and permeability. Nevertheless, the WSS assumes very low values at the end of the recirculation region. The regions where the vortex terminates are susceptible to atherosclerotic lesion as indicated by non-uniform hemodynamic indicators such as near-zero wall shear stress and elevated wall shear stress gradients as well as blood particle accumulation and deposition [38]. This explains why the peak of RRT assumes the trend shown in Fig. 9. With the increase of DOR, the recirculation zone ends further downstream the stenosis, and at 90% DOR this happens several diameters downstream the end of the stent, and is not visible in Fig. 9.

6. Discussion

The present paper completes the results presented in [13], where the fluid dynamics and the WSS are shown to be modified by the degree of DOR in the stent. The streamlines presented in [13] showed the presence of multiple recirculation regions downstream the residual stenosis, where the WSS is small and the Casson rheology plays a significant influence, as shown in Figs. 2-4. This conclusion confirms the importance of taking into account the non-Newtonian rheology of the blood, when studying the performances of coronary stents, in agreement with [11].

The results of the present paper concern the OD and RRT parameters, which give an estimation of the wall permeability to macromolecules, and, therefore, measure the likelihood of the wall to develop restenosis, and its position. The OD is an instantaneous variable while RRT takes into account the history of the flow. The results of Fig. 5 show that when the flow rate is small, the wall permeability is comparable for all the DOR investigated, except for 90%, where the abrupt increase in WSS reduce it considerably. Despite the asymmetry of the flow, the OD assumes a symmetric profile up to 45% DOR. For DOR greater than 45%, the OD shows a peak downstream the residual stenosis, which moves away from it as the DOR increases. This behavior has never been observed before at the best of the authors' knowledge. This result indicates that the permeability of the wall increases non-linearly with the DOR, and, in particular, that there is an abrupt increase above 45% DOR. This can imply that in these conditions a plant is prone to failure since this could lead to a restenosis development.

This conclusion is confirmed by the RRT profiles, which are symmetric from 0% to 45% DOR. Above 45% DOR, the RRT increases 3 times downstream the residual stenosis for a 52% DOR and more than 10 times for a 60% DOR. In analogy with the results of the OD, the peak of RRT move downstream for higher DOR. In conclusion, the results of OD and RRT show that both parameters give a good index of the wall permeability, despite the different definitions.

RRT is function of the OSI, shown in Fig. 8, which has a slightly unusual behavior as well. Normally, as shown for 0% DOR, Fig. 8a the OSI is higher around the stent, because the WSS is low and oscillatory. For a DOR equal to 52.5%, Fig. 8c, the highest OSI moves towards the centre of the intra-struts area, which corresponds to an abrupt increase of permeability. This means that the flow is constantly directed backwards

in proximity of the struts, and the region of inversion is moved towards the centre. This is probably the mechanism which favours the abrupt increase of wall permeability, because the presence of low and oscillatory WSS at the centre of the intra-struts area allows a higher intake of macromolecules, while for lower DOR this is not possible because it is prevented by the struts.

7. Conclusions

The present paper investigates the vascular wall permeability of a simplified coronary artery, subject to a stent plant. A smooth, symmetric residual stenosis is placed in the middle of the vessel and several degrees of residual stenosis (DOR), spanning from 0% to 90%, are investigated. As far as the blood viscosity is concerned, it tends to decrease, in correspondence to the necking, for an increasing degree of residual stenosis while, downstream the narrowing, the higher viscosity is concentrated close to the vessel wall. Therefore, the stenosis increases the erythrocytes concentration close to the wall and consequently the time which they spend close to the endothelium. This can lead to pathological conditions.

The numerical results of the OD and RRT agree in predicting an abrupt increase in wall permeability for DOR greater than 45%. The interpretation is that this phenomenon is due to the shift of the low and oscillatory WSS regions from the struts towards the centre of the mesh. This phenomenon is increased, for severe degrees of residual stenosis, especially at the end of the large recirculation region that is formed downstream the stenosis.

Acknowledgements

References

1. P.F. Davies, Flow-mediated endothelial mechano-transduction, *Physiological reviews* 75 (3) (1995) 519-560.

2. M.A. Gimbrone, G. García-Cardeña, Vascular endothelium, hemodynamics, and the pathobiology of atherosclerosis, *Cardiovascular Pathology* 22 (1) (2013) 9-15.

3. H.A. Himburg, D.M. Grzybowski, A.L. Hazel, J.A. LaMack, X.-M. Li, M.H. Friedman, Spatial comparison between wall shear stress measures and porcine arterial endothelial permeability, *American Journal of Physiology-Heart and Circulatory Physiology* 286 (5) (2004) H1916-H1922.

4. S.W. Lee, D.S. Smith, F. Loth, P.F. Fisher, and H.S. Bassiouny, Numerical and experimental simulation of transitional flow in a blood vessel junction, *Numerical Heat Transfer, Part A: Applications* 51 (1) (2007) 1-22.

5. M. Fu, W. Weng, and Y. Hongyong, Numerical simulation of the effects of blood perfusion, water diffusion, and vaporization on the skin temperature and burn injuries, *Numerical Heat Transfer, Part A: Applications* 65 (12) (2014) 1187-1203.

6. L. Lanoye, M. De Beule, C. Dewijngaert, P. Segers, P. Van Impe, and P. Verdonck, The Influence of the Strut Section Shape on the Flow Field in a Newly Stented Right Coronary Artery, *The 56th National Congress of Theoretical and Applied Mechanics, NCTAM, 2006.*

7. T. Seo, L.G. Schachter, A.I. Barakat, Computational study of fluid mechanical disturbance induced by endovascular stents, *Annals of biomedical engineering* 33 (4) (2005) 444-456.

8. J.F. LaDisa, D.A. Hettrick, L.E. Olson, I. Guler, E.R. Gross, T.T. Kress, J.R. Kersten, D.C. Warltier, P.S. Pagel, Stent implantation alters coronary artery hemodynamics and wall shear stress during maximal vasodilation, *Journal of Applied Physiology* 93 (6) (2002) 1939-1946.

9. N. Duraiswamy, J.M. Cesar, R.T. Schoephoerster, J.E. Moore Jr, Effects of stent geometry on local flow dynamics and resulting platelet deposition in an in vitro model, *Biorheology* 45 (5) (2008) 547-561.

10. F. Gori, A. Boghi, M. Amitrano, Three-dimensional numerical simulation of the fluid dynamics in a coronary stent, *ASME 2009 International Mechanical Engineering Congress and Exposition, American Society of Mechanical Engineers*, (2009) 407-411.

11. F. Gori, A. Boghi, Three-dimensional numerical simulation of non-newtonian blood in two coronary stents, *14th International Heat Transfer Conference, American Society of Mechanical Engineers*, (2010) 109-114.

12. Boghi, F. Gori, Numerical simulation of blood flow through different stents in stenosed and non-stenosed vessels, *Numerical Heat Transfer, Part A: Applications* 68 (3) (2015) 225-242.

13. Di Venuta, A. Boghi, F. Gori, Three-dimensional numerical simulation of a failed coronary stent implant at different degree of residual stenosis. Part I: fluid dynamics and shear stress on the vascular wall, *Numerical Heat Transfer*, submitted for publication.

14. M.H. Friedman, D.L. Fry, Arterial permeability dynamics and vascular disease, *Atherosclerosis* 104 (1) (1993) 189-194.

15. L.A. Clarke, Z. Mohri, P.D. Weinberg, High throughput en face mapping of arterial permeability using tile scanning confocal microscopy, *Atherosclerosis* 224 (2) (2012) 417-425.

16. C.D. Murray, The physiological principle of minimum work. I. the vascular system and the cost of blood volume, *Proceedings of the National Academy of Sciences* 12 (3) (1926) 207-214.

17. D.L. Fry, R.W. Mahley, K.H. Weisgraber, S. Oh, Simultaneous accumulation of evans blue dye and albumin in the canine aortic wall, *American Journal of Physiology-Heart and Circulatory Physiology* 233 (1) (1977) H66-H79.

18. F.B. Freedman, J.A. Johnson, Equilibrium and kinetic properties of the evans blue-albumin system, *American Journal of Physiology-Legacy Content* 216 (3) (1969) 675-681.

19. M. Packham, H. Rowsell, L. Jørgensen, J. Mustard, Localized protein accumulation in the wall of the aorta, *Experimental and molecular pathology* 7 (2) (1967) 214-232.

20. F.P. Bell, I.L. Adamson, C.J. Schwartz, Aortic endothelial permeability to albumin: focal and regional patterns of uptake and transmural distribution of 131i-albumin in the young pig, *Experimental and molecular pathology* 20 (1) (1974) 57-68.

21. D.L. Fry, Arotic evans blue dye accumulation: its measurement and interpretation, *American Journal of Physiology-Heart and Circulatory Physiology* 232 (2) (1977) H204-H222.

22. D.M. Martin, E.A. Murphy, F.J. Boyle, Computational fluid dynamics analysis of balloon-expandable coronary stents: influence of stent and vessel deformation, *Medical engineering & physics* 36 (8) (2014) 1047-1056.

23. F. Rikhtegar, C. Wyss, K. S. Stok, D. Poulikakos, R. Müller, V. Kurtcuoglu, Hemodynamics in coronary arteries with overlapping stents, *Journal of biomechanics* 47 (2) (2014) 505-511.

24. G. Lowe, A. Lee, A. Rumley, J. Price, F. Fowkes, Blood viscosity and risk of cardiovascular events: the Edinburgh artery study, *British journal of haematology* 96 (1) (1997) 168-173.

25. G. Sloop, A unifying theory of atherogenesis, *Medical hypotheses*, 47 (4) (1996) 321-325.

26. S. Robaina, C. Hitzman, K. Robertson, L. Davis, J.T. Lenz, Drug-eluting stent, US Patent 7,951,193 (May 31 2011).

27. Kastrati, J. Mehilli, J. Dirschinger, J. Pache, K. Ulm, H. Schühlen, M. Seyfarth, C. Schmitt, R. Blasini, F.-J. Neumann, et al., Restenosis after coronary placement of various stent types, *The American journal of cardiology* 87 (1) (2001) 34-39.

28. Fournier, Ronald L. *Basic transport phenomena in biomedical engineering*, pp. 122-139, CRC Press, 2011.

29. J.R. Womersley, Method for the calculation of velocity, rate of flow and viscous drag in arteries when the pressure gradient is known, *The Journal of physiology* 127 (3) (1955) 553.

30. K. Mukundakrishnan, P.S. Ayyaswamy, D. M. Eckmann, Finite-sized gas bubble motion in a blood vessel: Non-newtonian effects, *Physical Review* E 78 (3) (2008) 036303.

31. F. Gori, A. Boghi, Image-based computational fluid dynamics in a carotid artery, *ASME 2009 International Mechanical Engineering Congress and Exposition, American Society of Mechanical Engineers*, (2009) 123-128.

32. D.N. Ku, D.P. Giddens, C.K. Zarins, S. Glagov, Pulsatile flow and atherosclerosis in the human carotid bifurcation. positive correlation between plaque location and low oscillating shear stress, *Arteriosclerosis*, thrombosis, and vascular biology 5 (3) (1985) 293-302.

33. M. Malek, S.L. Alper, S. Izumo, Hemodynamic shear stress and its role in atherosclerosis, *Jama* 282 (21) (1999) 2035-2042.

34. Farb, D.K.Weber, F.D. Kolodgie, A.P. Burke, R. Virmani, Morphological predictors of restenosis after coronary stenting in humans, *Circulation* 105 (25) (2002) 2974-2980.

35. R.M. Berne, M.N. Levy, *Cardiovascular physiology*, Mosby, 1967.

36. L.-D. Jou, M.E. Mawad, Hemodynamic effect of neuroform stent on intimal hyperplasia and thrombus formation in a carotid aneurysm, *Medical engineering & physics* 33 (5) (2011) 573-580.

37. X. He, D.N. Ku, Pulsatile flow in the human left coronary artery bifurcation: average conditions, *Journal of biomechanical engineering* 118 (1) (1996) 74-82.

38. S. Hyun, C. Kleinstreuer, J. Archie, Hemodynamics analyses of arterial expansions with implications to thrombosis and restenosis, *Medical engineering & physics* 22 (1) (2000) 13-27.

Caption to Figures

*Figure 1 - Casson viscosity [Pa*s] versus shear rate [1/s].*

Figure 2 - Comparison of apparent viscosity at t=0.3s (diastole). DOR values: (a) 0%, (b) 30%, (c) 60%, (d) 90%.

Figure 3 - Comparison of apparent viscosity at t=0.4s. DOR values: (a) 0%, (b) 30%, (c) 60%, (d) 90%.

Figure 4 - Comparison of apparent viscosity at t=0.6s (systole). DOR values: (a) 0%, (b) 30%, (c) 60%, (d) 90%.
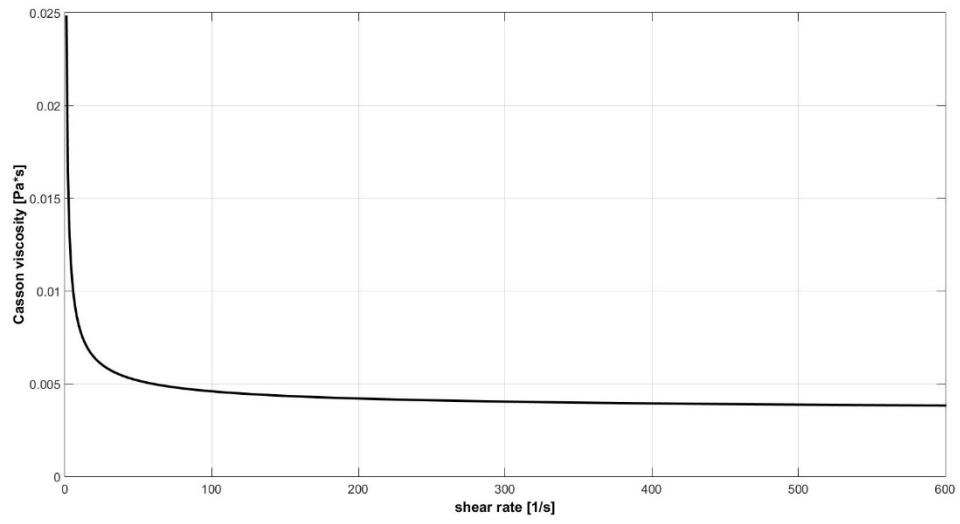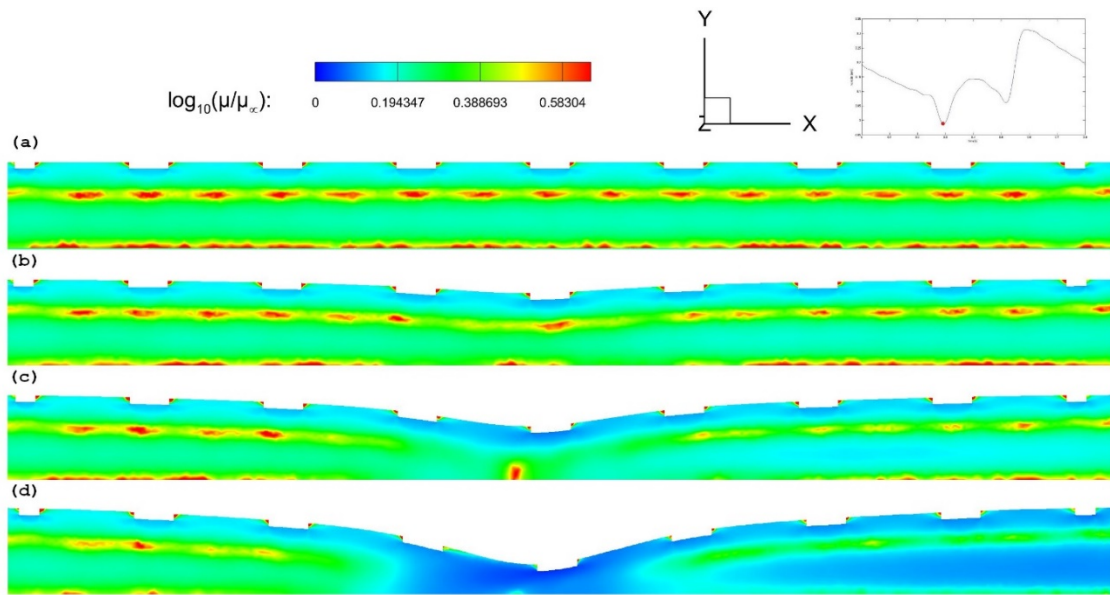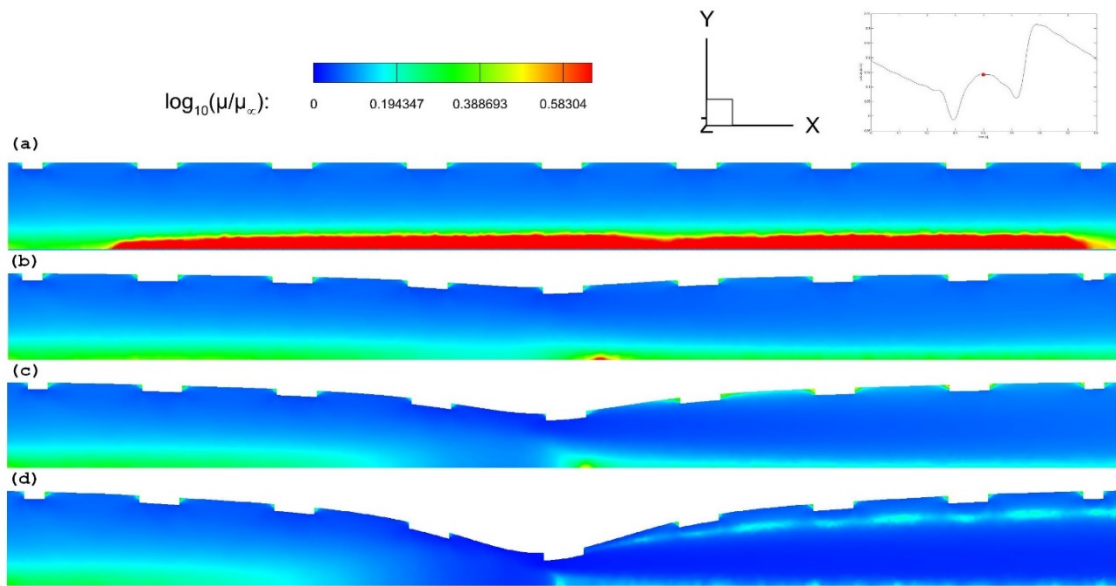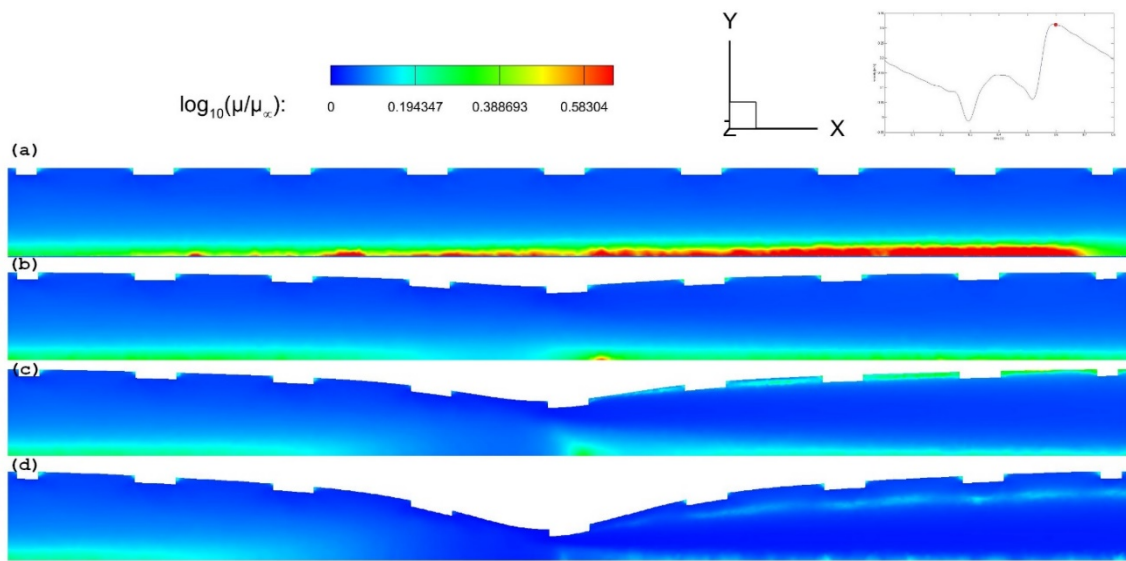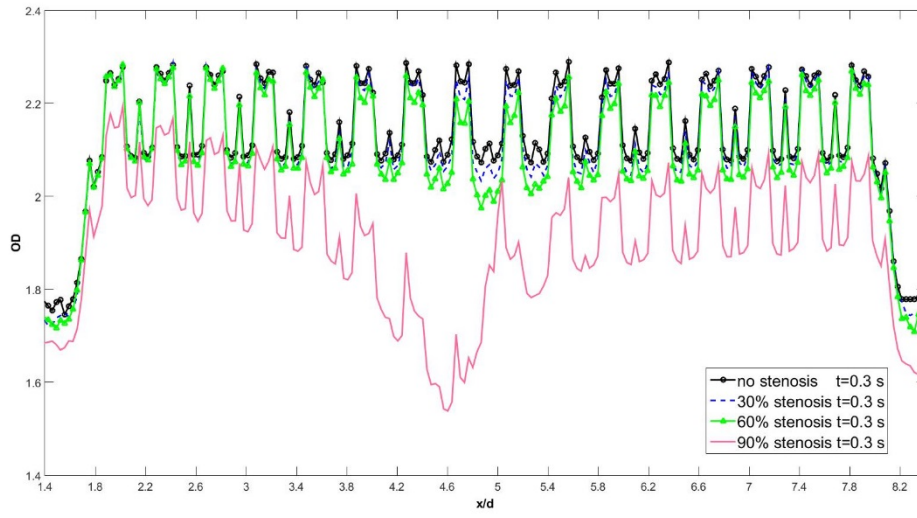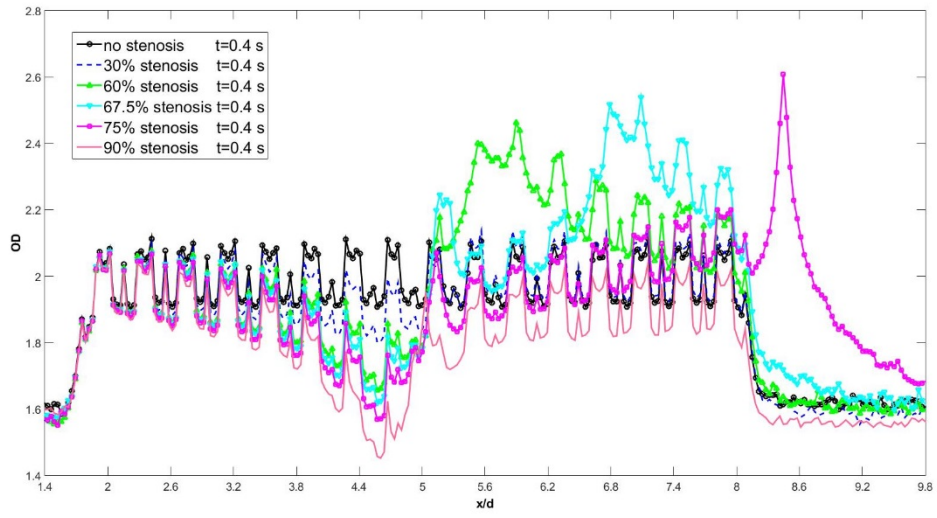
Figure 5 – OD versus axial length at t=0.3s (diastole).

Figure 6 – OD versus axial length at t=0.4s.

Figure 7 – OD versus axial length at t=0.6s (systole).

Figure 8 - OSI field for several DOR: (a) 0%, (b) 52.5% , (c) 60% , (d) 67.5% , (e) 90%.

Figure 9- RRT versus axial length.

Figure 1 - Casson viscosity [Pa*s] versus shear rate [1/s].

Figure 2 - Comparison of apparent viscosity at t=0.3s (diastole). DOR values: (a) 0%, (b) 30%, (c) 60%, (d) 90%.

Figure 3 - Comparison of apparent viscosity at t=0.4s. DOR values: (a) 0%, (b) 30%, (c) 60%, (d) 90%.

Figure 4 - Comparison of apparent viscosity at t=0.6s (systole). DOR values: (a) 0%, (b) 30%, (c) 60%, (d) 90%.

Figure 5 – OD versus axial length at t=0.3s (diastole).
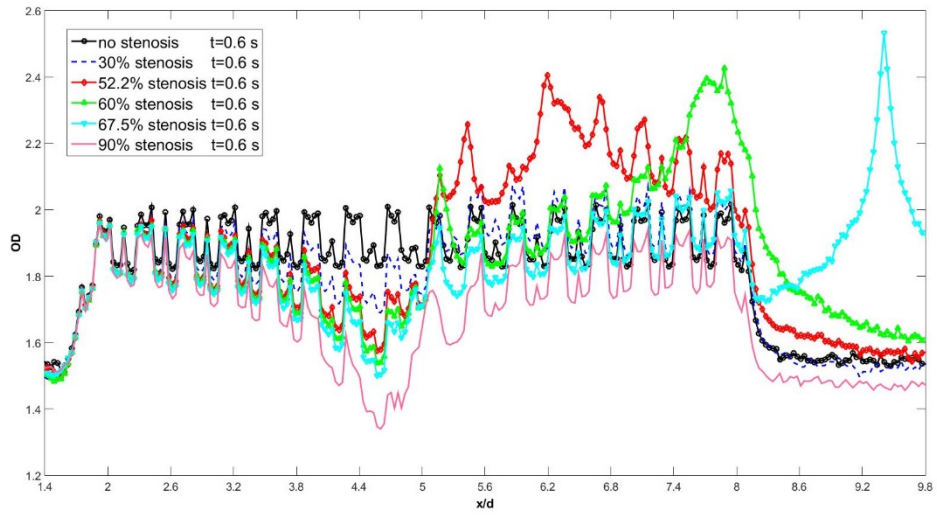
Figure 6 – OD versus axial length at t=0.4s.
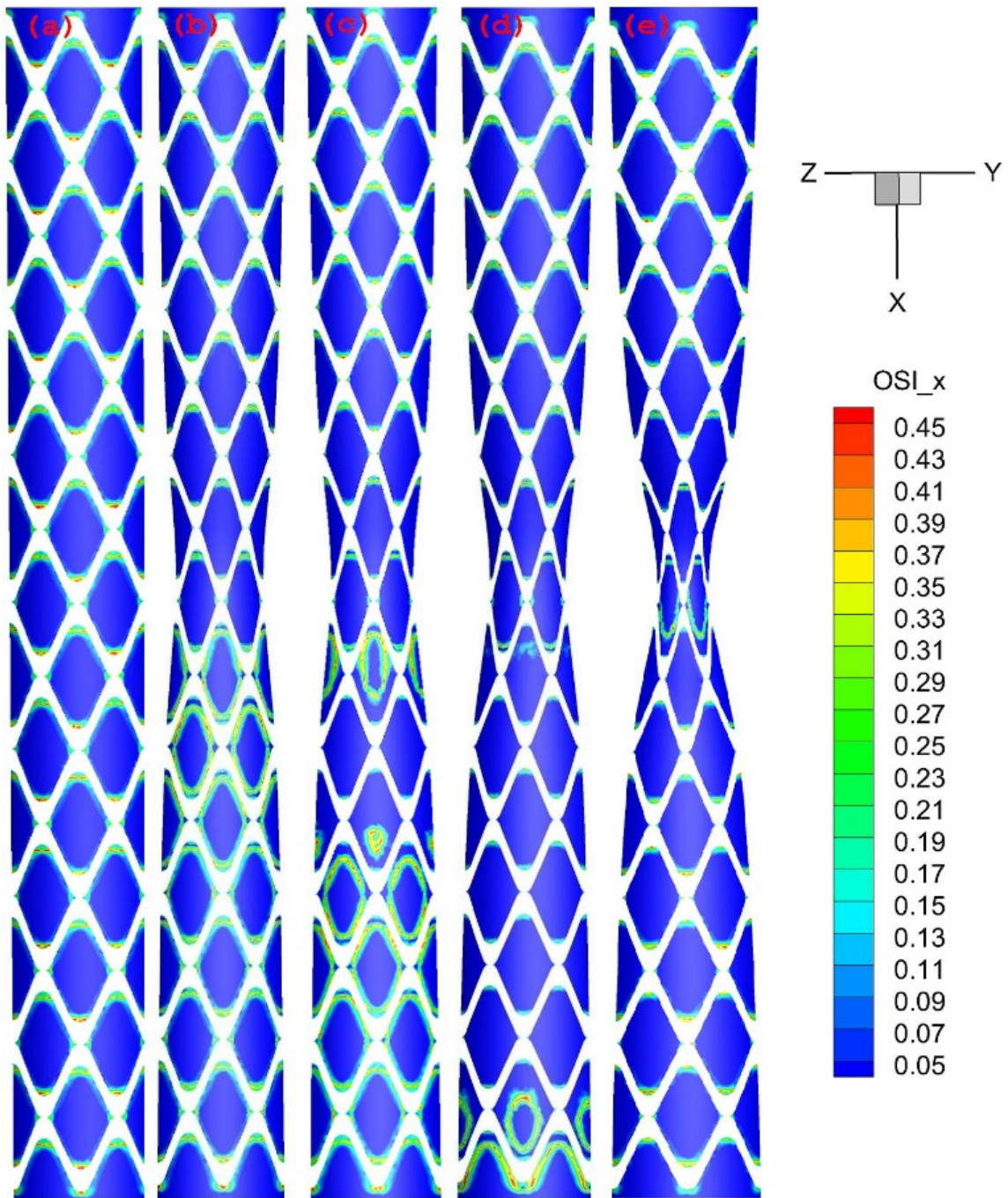
Figure 7 – OD versus axial length at t=0.6s (systole).

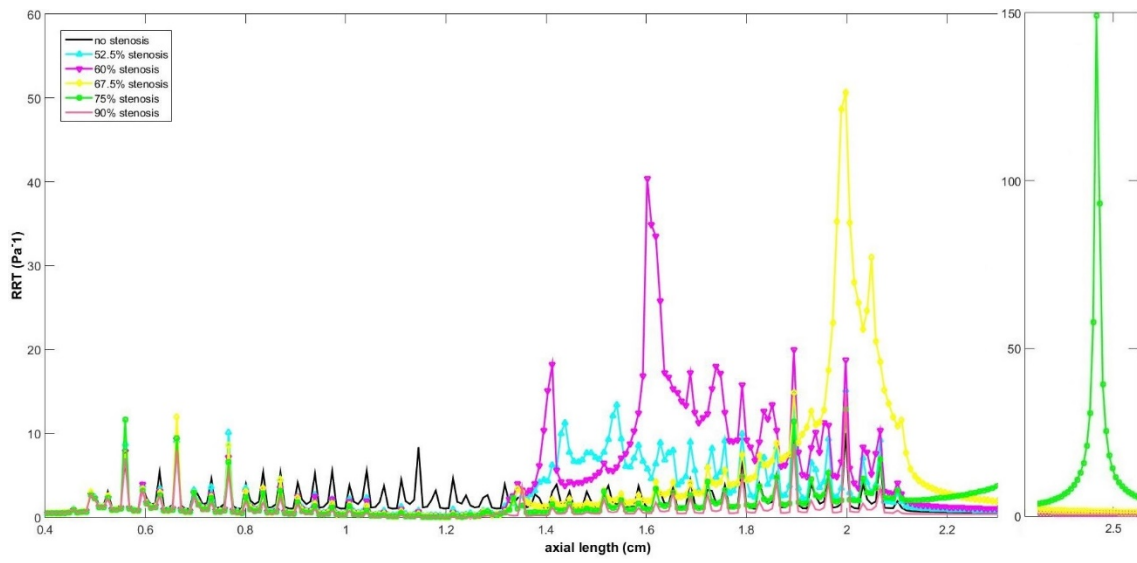*Figure 8 - OSI field for several DOR: (a) 0%, (b) 52.5% , (c) 60% , (d) 67.5% , (e) 90%.*

Figure 9- RRT versus axial length.